



Journal of Mining and Earth Sciences

Website: <http://jmes.humg.edu.vn>



Study of the urban heat island intensity using Landsat 8 in Da Nang in 2020



Thu Hoai Thi Trinh *, Tham Hong Thi Bui

Hanoi University of Natural Resources and Environment, Hanoi, Vietnam

ARTICLE INFO

Article history:

Received 19th July 2022

Revised 27th Dec. 2022

Accepted 31st Mar. 2023

Keywords:

Da Nang,
Landsat,
LST,
UHI intensity.

ABSTRACT

Monitoring spatiotemporal changes in land surface temperature in metropolitan areas is important to obtain the necessary information about environmental conditions and promote sustainable cities. Da Nang is a big city and is considered one of the tourist centers of Vietnam. Economic development and population growth lead to the expansion of urban land there. That affects the environment, especially resulting in the increase in surface temperature of the core city compared to the surrounding areas. The application of remote sensing data and techniques using thermal sensors for the estimation of land surface temperature and the formation of urban heat islands. This research aims to determine land surface temperature (LST) values and urban heat island (UHI) intensity distribution using Landsat 8 images. UHI is calculated in two steps: first, LST is calculated, and then the temperature threshold for UHI and non-UHI is determined by the mean and standard deviation statistics of LST in the study area. To compute the LST, two levels of data must be processed: the NIR and RED bands from level 1 and the thermal band from level 2. The results showed the temperature in Da Nang varies from 15.7-46.8 °C, with a significant regional temperature variance. The areas with high vegetation index had low temperatures while areas with low vegetation index had high temperatures. Non-UHI areas are present in areas with dense vegetation, dominated by Hoa Vang district and Son Tra peninsula. UHI is found in areas with temperatures more than or equal to 34.2 °C. The urban heat island has been taken place in the core of Da Nang, where the densely populated areas, industrial zones, airports, and landfill are located.

Copyright © 2023 Hanoi University of Mining and Geology. All rights reserved.

*Corresponding author

E - mail: tththu@hunre.edu.vn

DOI: 10.46326/JMES.2023.64(3).09

1. Introduction

Urban Heat Islands are one of the phenomena brought on by urbanization and climate change. This phenomenon occurs in urban areas with higher temperatures than in surrounding rural and suburban areas (Elmarakby et al., 2022; Taha, 1997). Urban zones that endure from UHIs bear the brunt of these cruel heat occasions and increase energy demand there (Kikegawa et al., 2006; Parker, 2021). As a result, UHI is probably one of the most important indicators of urban environmental conditions (Falahatkar et al., 2011; Niu et al., 2021). UHIs are determined using observations from meteorological stations or remote sensing data (Lai et al., 2018). Although in situ observations give accurate data, the number of stations and the spatial control of one station is limited for UHI mapping (Gao et al., 2013). Thus, using remote sensing with spatial continuity, wide coverage, and frequent data acquisition for UHI research is an attractive approach (de Faria Peres et al., 2018), and remote sensing has become an important method for monitoring and studying the urban heat island effect (Voogt and Oke, 2003; Weng, 2009).

Initial attempts to employ the advanced very high-resolution radiometer (AVHRR) and moderate resolution imaging spectrometer (MODIS), which can describe the general distribution of land surface thermal characteristics (Schwarz et al., 2011). The use of the medium-resolution of Landsat and Aster has become widespread in the study and description (Chen et al., 2006). In Vietnam, the development of thermal remote sensing provides a good solution to the flaw observed in conventional monitoring of urban heat islands. Many researchers have determined urban heat using remote sensing. For instance, (Pham and Watanabe, 2004) calculated the radiation temperature from ASTER remote sensing images in inner Hanoi in 2003. Le (2014) studied the land surface temperature distribution using multispectral images of Landsat in the dry season of 2007 and 2009 in Hanoi. Determined land surface temperature and the relationship between heat and urbanization factors. Assessing the effects of land-use types in surface urban heat islands for developing comfortable living in Hanoi

city (Thanh Hoan et al., 2018). The influences of land cover structure on surface urban heat islands: a case study of Ho Chi Minh, Vietnam (Le et al., 2020). Considering the previous studies, many researchers have determined land surface temperature and have investigated the effects of land use/ land cover change on LST in Hanoi and Ho Chi Minh city. Therefore, the purpose of this study is to fill a knowledge gap about the spatial pattern and intensity of UHI in Da Nang city. This paper will determine the UHI character, and the heat island characteristics of the Da Nang area based on the application of Landsat 8 images. LST surface temperature for the Da Nang area in 2020 using Fawzi's emissivity estimation formula (Puspita and Hadiyanti, 2022) as well as the thresholding to determine the UHI area according to the formula of (Elmarakby et al., 2022), hence, determine the characteristics of urban heat island in Da Nang area.

2. Study region and data

Da Nang is located in a coastal area of South Central Vietnam from 15°15'N to 16°40' N and between 107°17' E and 108°20' E with an area of 1284.9 km², of which Hoang Sa island district is 30.500 ha (Figure 1). The geographical condition of Da Nang has characteristics of physical land in the form of hills and coasts. High and steep mountains are concentrated in the West and northwest stretching to the sea, some low hills are interspersed with narrow coastal plains. The climate of Da Nang is tropical monsoon. The annual mean temperature is 29 °C, and the annual precipitation is 2.066 mm. The study area is within the mainland of Da Nang city.

In this study, LST and UHI are produced by the processing of Landsat 8 satellite imagery. Landsat 8 images were acquired on May 6 and 13, 2020, and September, 02 and 11, 2020 and are available from USGS for free (Table 1). The collected images were defined in both UTM zones 48 N and 49 N. Therefore, the images in the UTM 49 N must be reprojected to UTM 48 N. The thermal bands have a resolution of 100 m but have been resampled up to 30 m and used radiometric calibration to calibrate image data to radiance. After performing an atmospheric correction, two scene images covering the whole

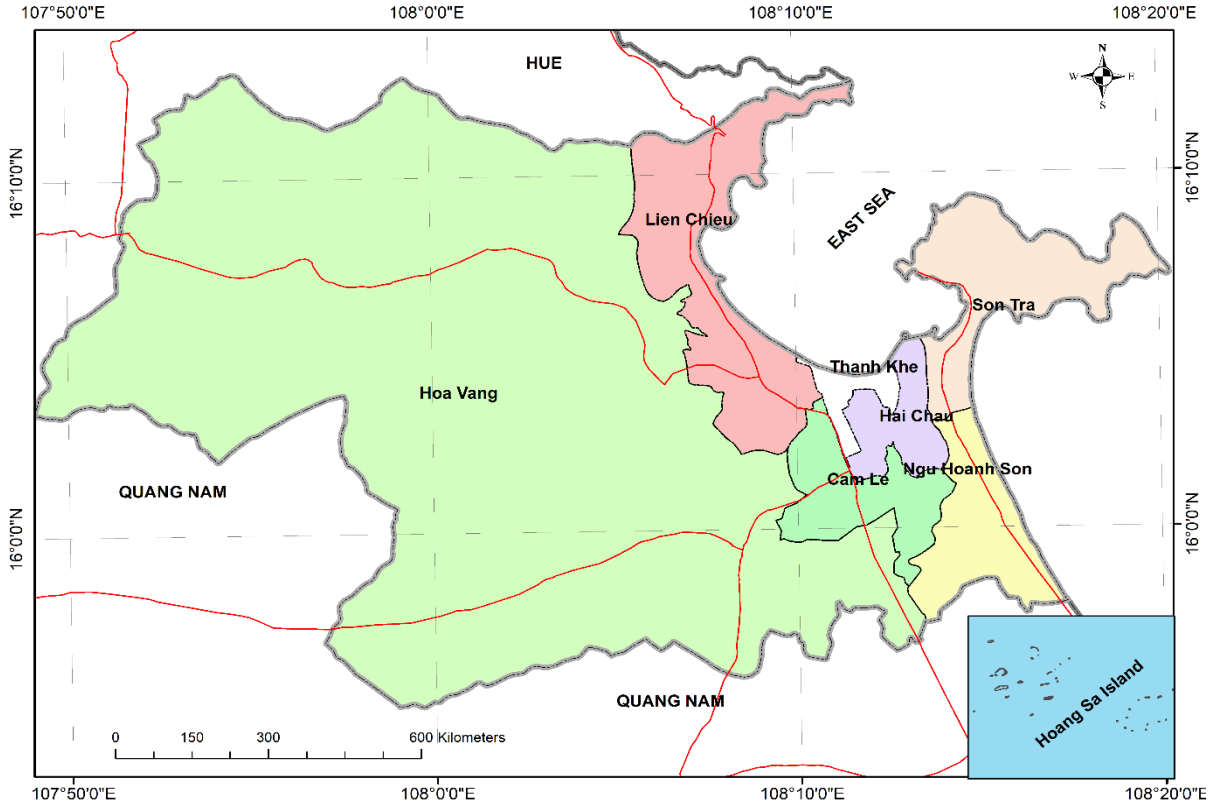


Figure 1. Study area.

area of Da Nang were created by combining each pair of Landsat 8 images in May and September to extract LST.

Table 1. Description of Landsat 8 datasets.

Date (Y-M-D)	UTC Time (hh:mm:ss)	Path/Row	Resolution (m)
2020-05-06	03:05:37	124/049	30
2020-05-13	03:11:47	125/049	30
2020-09-11	03:06:25	124/049	30
2020-09-02	03:12:32	125/049	30

3. Methods

It's necessary to process the two levels of data to determine UHI. The processing flow chart to determine UHI is depicted in Figure 2. NDVI is a simple graphical indicator that can be used to quantify vegetation by measuring the difference between near-infrared and red light. The NDVI value describes the vegetation density in the range from -1÷+1. NDVI values close to -1 represent non-vegetation areas or bodies of water. Positive values represent areas with sparse

to wide vegetation. The NDVI is calculated from these individual measurements in equation (1).

$$NDVI = \frac{NIR - RED}{NIR + RED} \quad (1)$$

Where: RED and NIR - stand for the spectral reflectance measurements acquired in the red (visible) and near-infrared regions, respectively.

The conversion from Digital Number (DN) to Top of Atmosphere (TOA) spectral radiance (L_λ). It is determined according to an Equation, using the thermal band.

$$L_\lambda = M_L \cdot Q_{cal} + A_L \quad (2)$$

Where: L_λ - the TOA spectral radiance; M_L - The band-specific multiplicative rescaling factor from the metadata (radiance_mult_band_x, where x is the band number); A_L - The band-specific additive rescaling factor from the metadata (radiance_add_band_x, where x is the band number); Q_{cal} - The quantized and calibrated standard product pixel value (DN).

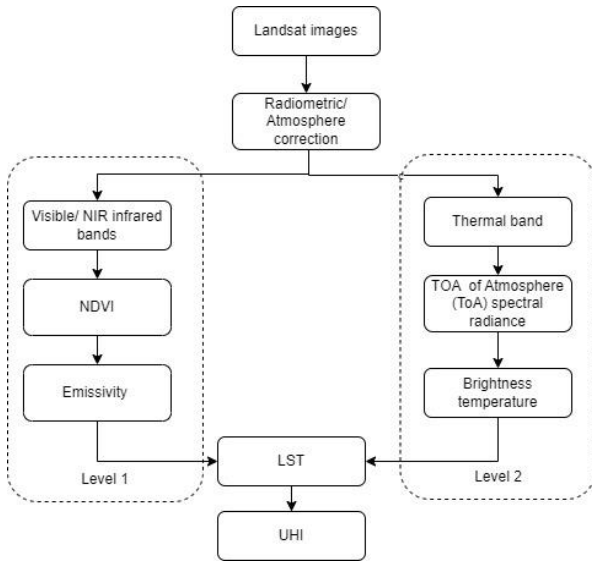


Figure 2. Flow chart of UHI estimation.

LST is determined through the interpretation of Landsat TM8 images in the following steps. The first step of the algorithm is that the thermal infrared radiation information is converted to a brightness temperature, using Equation (3) (Missions, 2016).

$$T = \frac{K_2}{\ln\left(\frac{K_1}{L_\lambda} + 1\right)} \quad (3)$$

Where: T - the mean brightness temperature in Kelvin; L_λ - the TOA spectral radiance; K_1 and K_2 - the thermal infrared (TIRS) bands 10 and 11 which can be found in the metadata file linked with the satellite image. And then, the brightness temperature can be calibrated to the LST via the surface emissivity (Avdan & Jovanovska, 2016).

$$LST = \frac{T}{1 + \left(\frac{\lambda T}{\rho}\right) \ln \varepsilon} \quad (4)$$

Where: T - the mean brightness temperature in Celsius; λ - the wavelength of emitted radiance.

$$\rho = \frac{h.c}{\sigma} = 1.438 * 10^{-2} mk = 14388 \mu mk$$

Where: σ - the Stefan - Boltzmann constant $1.38 * 10^{-23} \frac{J}{K}$, h - Planck's constant

$6.626 * 10^{-34} Js$; c - the velocity of the light $2.998 * 10^8 m/s$; ε - the emissivity calculated in (5).

The emissivity (ε) describes the radiative absorption ability of a surface in the loge wave radiation spectrum (Sobrino et al., 2008). Landsat thermal sensors detect and capture this radiation so that the temperature of the object could be acquired. The equation of emissivity is stated below (Puspita and Hadiyanti, 2022).

$$\varepsilon = \varepsilon_v P_v + \varepsilon_g (1 - P_v) + d_\varepsilon P_v (1 - P_v) \quad (5)$$

Where: ε_v - the emissivity of vegetation; ε_g - the emissivity of soil; d_ε - the effect of the geometry of the object and internal object reflection. In heterogeneous and rough surfaces, the effect is about 2%. In the equation, this value is multiplied by 4, so it resulted from 0, 06 as above.

P_v is the vegetation proportion that is calculated in equation (6).

$$P_v = \left[\frac{NDVI - NDVI_{\min}}{NDVI_{\max} - NDVI_{\min}} \right]^2 \quad (6)$$

Where: $NDVI_{\min}$ and $NDVI_{\max}$ - the minimum and maximum values obtained in the NDVI calculation, respectively.

In this study, UHI is defined by the following equation (Elmarakby et al., 2022):

$$\begin{aligned} LST &\geq \bar{T} \text{ for UHI area} \\ 0 < LST < \bar{T} &\text{ for non-UHI area or rural} \end{aligned} \quad (7)$$

Where: \bar{T} - a threshold temperature for UHI and non - UHI and is defined by the following equation:

$$\bar{T} = \mu + 1\alpha$$

Where: μ and α - the mean and standard deviation statistics of LST in the study area, respectively.

4. Results and discussion

The results of calculating NDVI show that the index values are in the range from $-0.657 \div 0.763$ and between $-0.912 \div 0.794$ in May and September 2020, respectively (Figure 3). In the NDVI index, a low value below -0.2 can be interpreted as a water

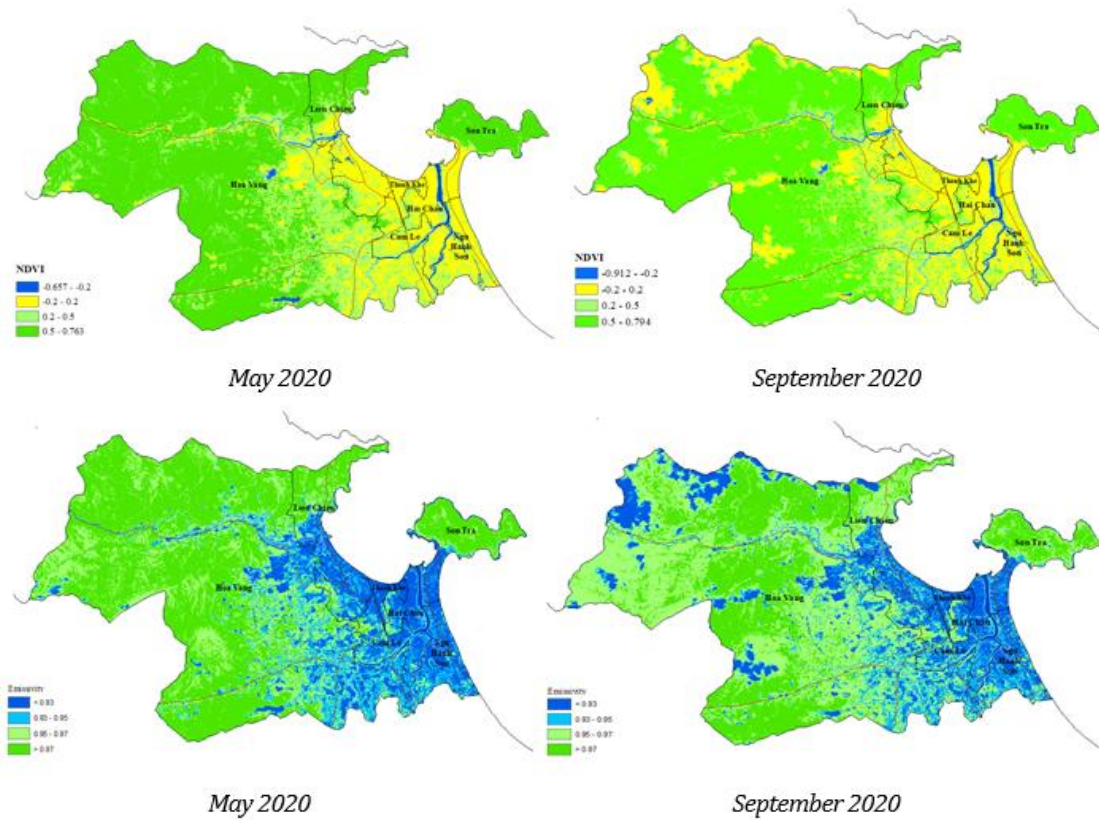


Figure 3. NDVI images of the study area; Emissivity images of the study area.

body, and a lower value than 0.2 in the form of bare land, dry land, or built-up areas, while NDVI values greater than 0.2 is vegetation. NDVI value of more than 0.7 is considered to be a primary forest. In general, the NDVI values are very similar in two-time points. However, September is the rainy season in Da Nang, so the lowest NDVI value at this time is -0.912.

The emissivity of a surface depends on many factors. The emissivity is influenced by both the material and the nature of the surface. The surface emissivity of the study area is determined according to formula (5) and is shown in Figure 3. Surface emissivity values in vegetated areas are often high, especially in areas with dense vegetation. Areas with high NDVI values corresponding to surface emissivity values are also high and vice versa, areas with low NDVI indexes have low surface emissivity such as Thanh Khe, Hai Chau, etc.

The existing correlation between the data obtained by the sensor and the weather station was used to evaluate the accuracy of this study. At national meteorological stations, air and land

surface temperature measurement data are collected. However, land surface temperature data is only gathered 4 times per day, at 0, 6, 13, and 19 in local time. As a result, there is no surface temperature data available at the same time as the image data. So, the evaluation will compare the data obtained from satellite images with the air temperature data obtained from the observation station using the formula below and the results of the evaluation are shown in Table 2.

$$MAE = \frac{1}{n} \sum |T_e - T_0|$$

Where: MAE - the mean absolute error; T_0 - the observed temperature ($^{\circ}C$); T_e - the estimated temperature ($^{\circ}C$); n - the number of monitoring stations or time observations.

Table 2. Comparison between land surface temperature and air temperature.

Date	T_0	T_e	Difference
May	36.9	34.0	- 2.9
Setemper	39.6	35.0	-4.6
MAE			3.75

The temperature obtained from satellite images is significantly higher than the temperature measured at the stations. This result is consistent with the findings of studies (Mildrexler et al., 2011; Nascimento et al. 2022). The difference between the land surface temperature and the air temperature is due to the transport of energy from the ground surface to the temperature probe of the weather station (1.5 m) (Nascimento et al. 2022). The temperature values observed at the stations near the land surface are still good data for validating the results.

Figure 5 shows the land surface temperature obtained from Landsat images. According to the LST images, the temperature of the city center is

significantly higher than that of the suburban and rural areas. Urban construction zones, which include residential areas, transportation roads, busy commercial areas, and industrial areas, are the locations with the highest temperatures of more than 30 degrees Celsius.

In Lien Chieu, Thanh Khe, Hai Chau, Cam Le, and Ngu Hanh, the common surface temperatures are in the range of 35÷40 °C, some places have temperatures between 40 and 45 °C and there are some places where the LST reaches nearly 47 °C in May 2020. In contrast, the LST corresponding to water surfaces, parks, green land, and cropland is relatively low in Son Tra or Hoa Vang districts.

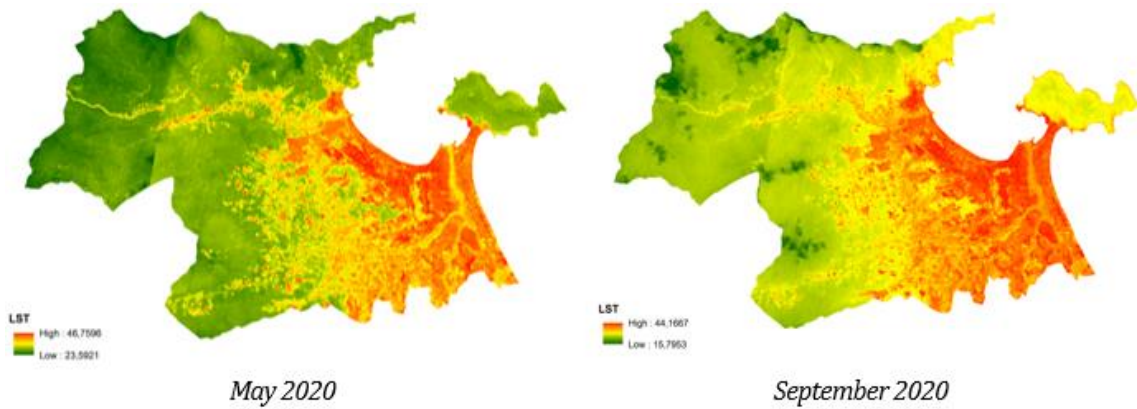


Figure 4. LST images of the study area.

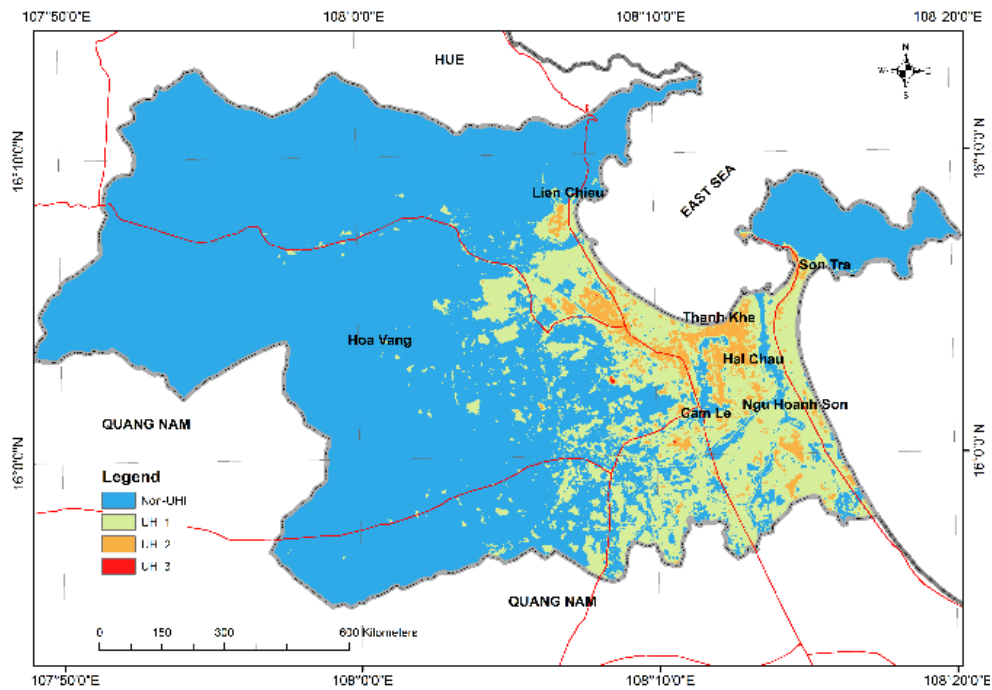


Figure 5. UHI map of the study area in 2020.

In this case, to determine the urban heat island of the area, we calculate the average temperature of two-time points and then find the mean and standard deviation according to raster data statistics in GIS. The results of the measurement of UHI in Da Nang, the mean temperature is 30.5 °C and the standard deviation of temperature is 3.7 °C.

Table 3 shows the threshold temperatures with 4 categories to give an overview of UHI in Da Nang and it is shown the UHI threshold value of a temperature is 34.2 °C. Heat islands are urbanized areas that experience higher temperatures than 34.2 °C to classify into three types based on 3.7 °C and occupy an area of 20372.1 ha, equivalent to 21.1% of the entire area. Table 3 lists the mean NDVI value for each UHI class. Non-UHI areas with LST values less than 34.2 °C have the highest mean NDVI values of 0.52. In contrast, UHI 3 regions have a land surface temperature greater than 41.6 °C, which is the highest temperature range corresponding to the lowest mean NDVI value of -0.13. These demonstrate that high temperatures correspond to low NDVI values and vice versa, indicating that NDVI values are inversely associated with temperature values. The results of the UHI classification presented in Figure 5 confirmed the spatial distribution and intensity of UHI. This study compared the LST in a particular UHI class with NDVI and actual land use/ land cover (LULC) to portray the significance of UHI processes in Da Nang. To extract land use/ land cover, 9 polygon samples (200x200 m) were selected from Google Earth images in May 2020 with the matching UHI classes property at the polygon centroid points. The results of these steps are shown in Table 3.

Table 3. LULC and UHI.

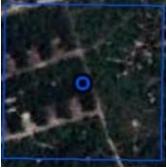
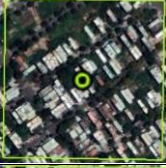
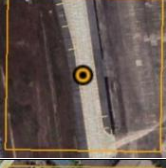
Class	UHI Intensity Value	Mean NDVI Value
Non-UHI	$LST < 34.2$	0.52
UHI 1	$34.2 \leq LST < 37.9$	0.07
UHI 2	$37.9 \leq LST < 41.6$	-0.04
UHI 3	$LST \geq 41.6$	-0.13

The map of UHI intensity displays classes with different colors. The highest UHI intensity is shown in red with a heat value greater than or equal to 41.6 °C and appears at the Khanh Son landfill site, industrial zone, and wastewater treatment pond. Khanh Son is the only landfill in Da Nang, receiving an average of 1, 100 tons of domestic waste per day, excluding medical and industrial waste, and is a hot spot for environmental pollution in the city (Xuan Ngo, 2019). The landfilling technique of waste treatment at Khanh Son is an outdated technology that generates metal emissions, groundwater contamination, air, and soil pollution, and it is a fire risk. Landfill heat is generated from the degradation of various waste types as a result of chemical and biological processes. Due to the heat generation process, the land surface temperature in the landfill area is often higher than in the surrounding areas. This has also been demonstrated in the studies of (Mahmood et al., 2016; Yan et al., 2014), waste disposal landfill usually has a higher LST concerning their surroundings by up to 10 °C depending on weather condition, the season, and the operating stage of the landfill. One piece of evidence demonstrates that, such as in India, Urban Heat Island (UHI) behavior has been observed in landfill environments (Plocoste et al. 2014).

The temperature of 37.9-41.6 °C is expressed as UHI 2 and is presented by orange. The distribution of this UHI intensity class is mostly concentrated in densely populated areas and industrial areas of the city such as Da Nang airport, Lien Chieu Industrial Park, Hoa Khanh Industrial Park, Hai Chau, Thanh Khe, etc. In general, the land use types commonly found at high temperatures are settlements, commercial buildings, and roads.

The distribution of UHI intensity class shows that most of the suburban areas of Da Nang city have low UHI values along with reduced construction density. And the non-UHI class is dominated by vegetative regions with NDVI mean values of 0.52 or higher, such as forests, orchards, groves, and crops.

Table 3. Classification of UHI intensity value.

UHI class	UHI overlaps Google earth image in May 2020	Coordinates of centroid points		Land use/Land cover
		Latitude	Longitude	
Non_UHI		16° 5'58.33"N	108° 4'4.39"E	Forest land
		16° 1'46.13"N	108°11'31.83"E	Agriculture/ Orchards, groves
		15°59'27.58"N	108°10'52.08"E	Agriculture/ Cropland
UHI 1		16° 0'17.87"N	108°13'1.78"E	Built-up/ Residential
		16° 3'49.38"N	108°14'19.74"E	Built-up/ Residential.
		16° 5'36.33"N	108° 4'50.33"E	Urban or built-up/roads and vacant land.
UHI 2		16° 2'13.11"N	108°12'9.96"E	Urban or built-up/ Transportation (Da nang airport).
		16° 4'53.66"N	108° 7'56.59"E	Urban or built-up/ Industrial area (Hoa Khanh industrial park).
		16° 4'7.28"N	108°12'34.33"E	Urban or built-up/ Commercial area.

UHI class	UHI overlaps Google earth image in May 2020	Coordinates of centroid points		Land use/Land cover
		Latitude	Longitude	
UHI 3		16° 2'29.56"N	108° 8'31.86"E	Landfill (Khanh Son Landfill).
		16° 0'26.41"N	108°10'35.26"E	Urban or built-up/ Industrial area (Hoa Cam industrial park).
		16° 1'49.75"N	108°13'3.20"E	Wastewater treatment pond.

5. Conclusions

Based on the Landsat 8 image of Danang, this study uses a threshold temperature to extract non-UHI and UHI spatial distribution and intensity. Two conclusions have been reached. (1) Da Nang exhibits the urban heat island phenomenon and the LST difference among different land covers is significant. The intensity of UHI is inversely proportional to the NDVI value. The high intensity of UHIs is concentrated in low-NDVI regions, which correspond to built-up, industrial, commercial, settlement, and road areas. Low UHI intensity, on the other hand, is prevalent in places with high NDVI values, such as forests, orchards, groves, and crops. (2) In Danang, urban heat islands do not only occur in densely populated areas, or industrial areas but also occur in landfills where the UHI intensity is strongest.

Author contributions

Thu Hoai Thi Trinh – methodology, design the analysis, writing manuscript; Tham Hong Thi Bui - collecting the data and analysis, editing the manuscript.

References

Avdan, U., Jovanovska, G. (2016). Algorithm for automated mapping of land surface temperature using LANDSAT 8 satellite data. *Journal of sensors*, 2016.

Chen, X. L., Zhao, H. M., Li, P. X., & Yin, Z. Y. (2006). Remote sensing image-based analysis of the relationship between urban heat island and land use/cover changes. *Remote sensing of environment*, 104(2), 133-146.

de Faria Peres, L., de Lucena, A. J., Rotunno Filho, O. C., & de Almeida França, J. R. (2018). The urban heat island in Rio de Janeiro, Brazil, in the last 30 years using remote sensing data. *International journal of applied earth observation and geoinformation*, 64, 104-116.

Elmarakby, E., Khalifa, M., Elshater, A., & Afifi, S. (2022). Tailored methods for mapping urban heat islands in Greater Cairo Region. *Ain Shams Engineering Journal*, 13(2), 101545.

Falahatkar, S., Hosseini, S. M., & Soffianian, A. R. (2011). The relationship between land cover changes and spatial-temporal dynamics of land surface temperature. *Indian Journal of Science and Technology*, 4(2), 76-81.

Gao, C., Jiang, X., Li, Z. L., & Nerry, F. (2013). Comparison of the Thermal Sensors of SEVIRI and MODIS for LST Mapping. *Thermal Infrared Remote Sensing: Sensors, Methods, Applications*, 233-252.

Kikegawa, Y., Genchi, Y., Kondo, H., & Hanaki, K. (2006). Impacts of city-block-scale countermeasures against urban heat-island phenomena upon a building's energy-

- consumption for air-conditioning. *Applied Energy*, 83(6), 649-668.
- Lai, J., Zhan, W., Huang, F., Voogt, J., Bechtel, B., Allen, M., ... & Du, P. (2018). Identification of typical diurnal patterns for clear-sky climatology of surface urban heat islands. *Remote sensing of environment*, 217, 203-220.
- Le, H. T. (2014). Studies of land surface temperature distribution using multispectral image Landsat. *Vietnam Journal of Earth sciences*, 36(1), 82-89.
- Le, H. T. T., Doan, N. D., Huynh, L. T., Nguyen, T. T. T., Nguyen, H. N. T., Luu, T. T. T., ... & Le, N. T. (2020). The Influences of Landcover structure on surface urban heat islands: A case study of Ho Chi Minh, Vietnam. *Journal of Mining and Earth Sciences Vol*, 61(2), 76-85.
- Mahmood, K., Batool, S. A., & Chaudhry, M. N. (2016). Studying bio-thermal effects at and around MSW dumps using Satellite Remote Sensing and GIS. *Waste Management*, 55, 118-128.
- Mildrexler, D. J., Zhao, M., & Running, S. W. (2011). A global comparison between station air temperatures and MODIS land surface temperatures reveals the cooling role of forests. *Journal of Geophysical Research: Biogeosciences*, 116(G3).
- Missions, L. (2016). Using the USGS Landsat8 product. *US Department of the Interior-US Geological Survey-NASA*.
- Nascimento, A. C. L., Galvani, E., Gobo, J. P. A., & Wollmann, C. A. (2022). Comparison between Air Temperature and Land Surface Temperature for the City of São Paulo, Brazil. *Atmosphere*, 13(3), 491.
- Niu, L., Zhang, Z., Peng, Z., Liang, Y., Liu, M., Jiang, Y. & Tang, R. (2021). Identifying surface urban heat island drivers and their spatial heterogeneity in China's 281 cities: An empirical study based on multiscale geographically weighted regression. *Remote Sensing*, 13(21), 4428.
- Parker, J. (2021). The Leeds urban heat island and its implications for energy use and thermal comfort. *Energy and Buildings*, 235, 110636.
- Pham, V. C., Watanabe, H. (2004). Use of Thermal Infrared Channels of ASTER to evaluate the Land Surface Temperature Changes of an Urban Area in Hanoi, Vietnam. *Japan-Vietnam Geoinformatics Consortium*, 19 Le Thanh Tong Campus, Hanoi University of Science, Conference Hall, Hanoi, Vietnam <http://gisws.media.osaka-cu.ac.jp/gisideas04/>.
- Plocoste, T., Jacoby-Koaly, S., Molinié, J., & Petit, R. (2014). Evidence of the effect of an urban heat island on air quality near a landfill. *Urban climate*, 10, 745-757.
- Puspita, B. D., & Hadiyanti, A. (2022). Measuring Urban Heat Islands Using Landsat 8 TIRS and Investigating the Variety of Landuse Proportion in Yogyakarta City. In *Proceeding International Conference on Religion, Science and Education* (Vol. 1, pp. 595-603).
- Schwarz, N., Lautenbach, S., & Seppelt, R. (2011). Exploring indicators for quantifying surface urban heat islands of European cities with MODIS land surface temperatures. *Remote Sensing of Environment*, 115(12), 3175-3186.
- Sobrino, J. A., Jiménez-Muñoz, J. C., Sòria, G., Romaguera, M., Guanter, L., Moreno, J., ... & Martínez, P. (2008). Land surface emissivity retrieval from different VNIR and TIR sensors. *IEEE transactions on geoscience and remote sensing*, 46(2), 316-327.
- Taha, H. (1997). Urban climates and heat islands: albedo, evapotranspiration, and anthropogenic heat. *Energy and buildings*, 25(2), 99-103.
- Thanh Hoan, N., Liou, Y. A., Nguyen, K. A., Sharma, R. C., Tran, D. P., Liou, C. L., & Cham, D. D. (2018). Assessing the effects of land-use types in surface urban heat islands for developing comfortable living in Hanoi City. *Remote Sensing*, 10(12), 1965.
- Voogt, J. A., & Oke, T. R. (2003). Thermal remote sensing of urban climates. *Remote sensing of environment*, 86(3), 370-384.
- Weng, Q. (2009). Thermal infrared remote sensing for urban climate and environmental studies: Methods, applications, and trends. *ISPRS Journal of photogrammetry and remote sensing*, 64(4), 335-344.

Xuan Ngo (2019). Da Nang: Focus on solving pollution at Khanh Son landfill. *Environment Magazine*.

Yan, W. Y., Mahendrarajah, P., Shaker, A., Faisal, K., Luong, R., & Al-Ahmad, M. (2014). Analysis of

multi-temporal landsat satellite images for monitoring land surface temperature of municipal solid waste disposal sites. *Environmental monitoring and assessment*, 186, 8161-8173.